Lipid14: The Amber Lipid Force Field

Callum J. Dickson,[§,†] Benjamin D. Madej,[‡,±,†] Åge A. Skjevik,[‡,¶] Robin M. Betz,[‡] Knut Teigen,[¶] Ian R. Gould,*[,§] and Ross C. Walker*[,‡,±]

[§]Department of Chemistry and Institute of Chemical Biology, Imperial College London, South Kensington SW7 2AZ, United Kingdom

[‡]San Diego Supercomputer Center, University of California San Diego, 9500 Gilman Drive MC0505, La Jolla, California 92093-0505, United States

[¶]Department of Biomedicine, University of Bergen, N-5009 Bergen, Norway

[±]Department of Chemistry and Biochemistry, University of California San Diego, 9500 Gilman Drive MC0505, La Jolla, California 92093-0505, United States

Ⓢ Supporting Information

ABSTRACT: The AMBER lipid force field has been updated to create Lipid14, allowing tensionless simulation of a number of lipid types with the AMBER MD package. The modular nature of this force field allows numerous combinations of head and tail groups to create different lipid types, enabling the easy insertion of new lipid species. The Lennard-Jones and torsion parameters of both the head and tail groups have been revised and updated partial charges calculated. The force field has been validated by simulating bilayers of six different lipid types for a total of 0.5 μs each without applying a surface tension; with favorable comparison to experiment for properties such as area per lipid, volume per lipid, bilayer thickness, NMR order parameters, scattering data, and lipid lateral diffusion. As the derivation of this force field is consistent with the AMBER development philosophy, Lipid14 is compatible with the AMBER protein, nucleic acid, carbohydrate, and small molecule force fields.
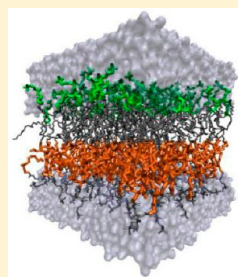
INTRODUCTION

Membranes are integral components of the cell, separating intracellular compartments from the cytosol. Such membranes consist of a back-to-back arrangement of lipid molecules, driven into a bilayer structure by the hydrophobic effect, leaving the polar lipid head groups exposed to water, and bringing the nonpolar lipid tail groups together. The composition of cell membranes is complex, with constituent species including, but not limited to, saturated and unsaturated PC and PE lipids, sphingomyelin and cholesterol, which serve as a matrix in which membrane proteins may reside.[1] Cell membranes possess functions such as regulating transport in to and out of the cell and modulating the activity of membrane embedded ion channels and proteins.[2,3]

In order to probe the many roles of membranes in the cell, membrane structures are studied experimentally using techniques such as X-ray and neutron scattering, IR/Raman, and NMR spectroscopy.[4,5] To gain atomic-level resolution, however, membranes may also be simulated computationally using molecular dynamics (MD). The validity of results obtained using MD methods depends, to a large extent, on the potential energy function, or force field, that is used.

Membranes can be simulated using all-atom, united-atom, or coarse-grained models,[6−13] with the increasing simplicity of each representation allowing access to larger models and longer time scales, at the expense of atomic detail. All-atom models may be preferred for bilayer simulations due to their ability to reproduce NMR order parameters and easy combination with all-atom protein, nucleic acid, carbohydrate, and small molecule

force fields.[14−16] One such MD software package that includes all-atom simulations is AMBER,[17,18] which contains extensively validated protein, nucleic, carbohydrate, and small molecule force fields. The AMBER simulation code has also been ported to NVIDIA GPU cards, making simulation speeds in excess of 100 ns per day possible for systems of 25,000 to 50,000 atoms, with systems of up to 4 million atoms possible on the latest generation hardware.[19−21] Although the AMBER force field suite includes numerous different species of biological interest, parameters for the simulation of lipids have traditionally been lacking. Recently the Lipid11 framework was introduced, which is a modular lipid AMBER force field, allowing the simulation of a number of lipids via the combination of different head and tail groups.[22] Lipid11 used force field parameters predominantly taken directly from the General Amber Force Field (GAFF).[16] Although previous studies found some success in simulating lipid bilayers using GAFF parameters,[23−25] longer time scale simulations required a surface tension term in order to keep a bilayer in the correct phase at a given temperature.[22]

In this paper we draw inspiration from previous work[26] to update Lipid11 headgroup and tail group charges and parameters to enable proper tensionless simulation of lipid bilayers, thereby creating a modular AMBER lipid force field. Lennard-Jones and torsion parameters are revised, while charges are derived according to the standard AMBER convention, as was implemented in Lipid11 with minor

improvements in sampling for Lipid14. As such, the resulting parameters are expected to be compatible with other force fields in the AMBER package.

We validate these parameters for a number of PC and PE lipids — six different lipid types are simulated for a total of 500 ns each, with resulting area per lipid, volume per lipid, isothermal compressibility, NMR order parameters, scattering form factors, and lipid lateral diffusion finding favorable comparison to experiment, particularly for PC lipids. We also assess the conformation of the lipid tails by examining the number of rotamers and rotamer sequences. To fully test the reproducibility of the results, a number of additional GPU and CPU runs were performed. We believe that these parameters will be transferable thus allowing the easy insertion of new lipid types into Lipid14 owing to the modular nature of the force field. The Lipid14 force field will be released with the upcoming AmberTools14. It is our intention to incorporate support for additional lipid types and other residues commonly found in bilayers, as part of the upcoming release. The derivation of these parameters will be described elsewhere.

■ PARAMETERIZATION STRATEGY

Generation of Lipid14 Parameters. Lipid14 aims to extend the Lipid11[22] framework to allow accurate, tensionless simulation of numerous lipid types via a modular lipid force field. Bond, angle, torsion, and Lennard-Jones (LJ) parameters in Lipid11 were taken directly from the General Amber Force Field (GAFF).[16] Although bond and angle parameters should not require updating, it was expected that torsion and LJ parameters would need modification to realize this aim.

Previous work on lipid simulation with AMBER indicated that the Lennard-Jones and torsion parameters of the lipid aliphatic tails are intricately linked to the ability of the force field to reproduce experimentally observed bilayer properties.[26] Indeed, the majority of all-atom lipid force field parameterization has involved the modification of the LJ and torsion parameters used to model the aliphatic tail regions of the lipids.[7,8,10,27]

Simulating a box of 144 pentadecane chains using the standard GAFF LJ and torsion parameters at constant pressure (1 atm) and temperature (298.15 K) causes the hydrocarbon chains to 'freeze' into a crystalline state in under 2 ns (see Figure 1). Such a scenario has previously been observed by Klauda et al. using a box of tetradecane molecules and the AMBER99 force field.[28] Consequently, the calculated density and heat of vaporization are much higher and the diffusion much lower than experiment.

In light of this, LJ and torsion parameters were modified to reproduce the experimental density (ρ) and heat of vaporization (ΔH_{vap}) of alkanes covering a range of chain lengths. Given that both the torsion and LJ parameters affected the simulated ρ and ΔH_{vap}, these parameters were altered simultaneously, with the $CH_2-CH_2-CH_2-CH_2$ torsion being fitted to ab initio data using Paramfit.[17,29] Satisfactory agreement was found by modifying only the LJ parameters of the hydrogen atom on the alkane chains.

The modified LJ and torsion parameters were tested by examining the density ρ, heat of vaporization ΔH_{vap}, the diffusion D, the ^{13}C NMR T_1 relaxation times, and the *trans/ gauche* conformer populations of a selection of hydrocarbon chains.

The parameters of the ester linkage region connecting headgroup and tail residues in the lipids were then examined
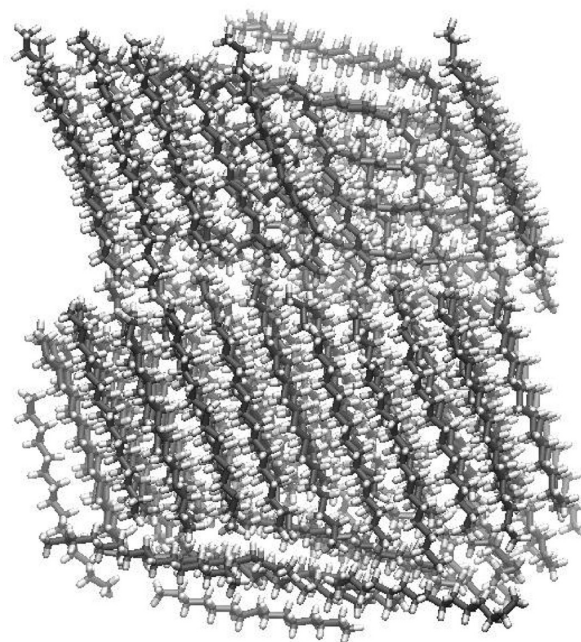
Figure 1. A box of 144 pentadecane molecules simulated in the NPT ensemble at 298.15 K using the General Amber Force Field[16] to model the carbon chains.

using methyl acetate as a model compound. The density and heat of vaporization of methyl acetate were calculated and ΔH_{vap} found to be in poor agreement with experiment. Hence the Lennard-Jones parameters of a number of atoms in this region were also adjusted until better agreement with experiment was achieved.

Once optimal hydrocarbon and glycerol parameters were identified, attention turned to the lipid partial charges. The Lipid11 force field used a capping procedure, separating the lipid head and tail groups into 'residues', thus creating a modular lipid force field.[22] The standard AMBER RESP protocol[30] was used to generate partial charges from quantum mechanical (QM) optimized structures, using six different orientations of a single conformation.

This methodology was kept for Lipid14. However, in line with other all-atom lipid force field parameterizations,[10,31] a greater number of conformations were used per residue (twenty-five headgroup conformations, fifty tail conformations), with the partial charges calculated as an average over all conformations. The head and tail group starting structures were extracted from previous in-house bilayer simulations. This allows one to obtain Boltzmann weighted charges, introducing a temperature dependence.[10,31] The electrostatic potential (ESP) was calculated directly from the conformations extracted from a bilayer simulation, with no QM optimization performed on those structures. Charges were derived using the standard AMBER RESP protocol (at the HF/6-31G* level in gas phase).[30]

Finally, on identification of appropriate LJ parameters and calculation of lipid partial charges, torsions involving the ester linkage in the glycerol region were fitted to QM scans performed on a capped lauroyl (LA) tail moiety.

Hydrocarbon Tail Parameters. The alkane $CH_2-CH_2-CH_2-CH_2$ torsion potential was refitted using torsion scans performed on hexane and octane molecules using an estimation

B

dx.doi.org/10.1021/ct4010307 | J. Chem. Theory Comput. XXXX, XXX, XXX−XXX

Table 1. Modification of LJ and Torsion Parameters of Alkane Chains

	LJ parameters			$CH_2-CH_2-CH_2-CH_2$ torsion		
	atom type	radius R (Å)	well-depth ε (kcal mol^{-1})	force constant PK (kcal mol^{-1})	periodicity PN	phase (deg)
Lipid11	cA	1.9080	0.1094	0.20	1	180
	hA	1.4870	0.0157	0.25	2	180
				0.18	3	0
Lipid14	cD	1.9080	0.1094	0.3112	1	180
	hL	1.4600	0.0100	−0.1233	2	180
				0.1149	3	0
				−0.2199	4	0
				0.2170	5	0

of the CCSD(T)/cc-pVQZ level of theory via the HM-IE relation[32]

$$
\begin{aligned}
E^{\text{conf}}&[\text{CCSD(T)/LBS}] \\
&= E^{\text{conf}}[\text{CCSD(T)/SBS}] + (E^{\text{conf}}[\text{CCSD(T)/LBS}] \\
&\quad - E^{\text{conf}}[\text{CCSD(T)/SBS}]) \\
&\cong E^{\text{conf}}[\text{CCSD(T)/SBS}] + (E^{\text{conf}}[\text{MP2/LBS}] \\
&\quad - E^{\text{conf}}[\text{MP2/SBS}]) \equiv E^{\text{conf}}[\text{MP2: CC}]
\end{aligned}
$$

where the small basis set (SBS) was cc-pVDZ and the large basis set (LBS) was cc-pVQZ. Consequently molecules were optimized at the MP2/cc-pVDZ level before single-point energy calculations were performed at the CCSD(T)/cc-pVDZ and MP2/cc-pVQZ levels. In order to obtain a representative torsion fit, it was ensured that torsion scans, conducted at increments of 15°, included local minima of hexane and octane.[10,28,33] The Paramfit program of Amber-Tools13[17,29] was used to perform a multiple molecule weighted torsion fit, with the *tgt* local minima of hexane and *tgttt* local minima of octane given a weighting of 10, all other local minima given a weighting of 4 and *cis* conformers given a weighting of 0.1; all other structures were assigned a weighting of 1. These weighting values have previously given good results for alkane torsion fitting.[33] Torsions were fitted using a genetic algorithm.

Lennard-Jones parameters were modified while simultaneously refitting the torsion parameters (see Table 1) until good agreement with experiment was achieved for heats of vaporization and densities for a range of alkane chains. These properties were monitored by performing liquid phase simulations of pentane, hexane, heptane, octane, decane, tridecane, and pentadecane. The alkane trajectories also enabled the calculation of a number of other properties for comparison to experiment.

Initial charges for each hydrocarbon chain were generated using the standard AMBER RESP protocol (optimization and calculation of the ESP at HF/6-31G* level in gas phase). A box of 288 (pentane, hexane and heptane) or 144 (octane, decane, tridecane, and pentadecane) molecules were then simulated in the liquid phase at 298.15 K for 10 ns using updated LJ and torsion parameters. From each liquid phase simulation, fifty different chains were extracted and used for the charge calculation, with the ESP calculated directly from each structure at the HF/6-31G* level, and partial charges derived using the RESP fitting procedure. Charges were taken as an average over all fifty RESP fits.

The heat of vaporization was calculated according to[34]

$$
\Delta H_{\text{vap}} = E_{\text{pot}}(g) - E_{\text{pot}}(l) + RT \tag{1}
$$

where $E_{\text{pot}}(g)$ is the average molecular potential energy in the gas phase, $E_{\text{pot}}(l)$ is the average molecular potential energy in the liquid phase, R is the gas constant, and T is temperature. In order to calculate the heat of vaporization, two simulations were performed in a similar manner to previous work.[26] A gas phase simulation consisting of a single alkane molecule was run for 10 ns equilibration and 50 ns production under the NPT ensemble, at a temperature of 298.15 K to obtain $E_{\text{pot}}(g)$. A liquid phase simulation consisting of a box of either 144 or 288 chains, run under the NPT ensemble with periodic boundary conditions using particle mesh Ewald to treat long-range electrostatics[35] and a real space cutoff of 10 Å, was also performed for 60 ns with the first 10 ns removed for equilibration to obtain $E_{\text{pot}}(l)$. The temperature was maintained at 298.15 K using Langevin dynamics and a collision frequency of 5 ps^{-1}. Bonds involving hydrogen were constrained using the SHAKE algorithm.[36] Pressure regulation was achieved with isotropic position scaling, a Berendsen barostat,[37] and a pressure relaxation time of 1 ps. The system was heated from 0 to 298.15 K over 20 ps, with a force constant of 20 kcal/mol/Å^2 restraining the chains. This restraint was gradually decreased to 10, 5 and finally 1 kcal/mol/Å^2 and the system simulated for 20 ps at each value of the force constant. The heat of vaporization was then calculated using eq 1, with results reported as block averages ± standard deviation using five equal blocks of 10 ns.

By reducing the van der Waals radius (R) and well-depth (ε) of the alkane hydrogen atom type while simultaneously correcting the torsion fit, satisfactory agreement with experiment was achieved for ρ and ΔH_{vap} for the alkane chains under study.

Three torsion scans about the C=C double bond were also performed on a *cis*-5-decene molecule using the MP2:CC extrapolation method − see Figure 2. When fitting the C=C double bond torsions, the LJ parameters of the alkene hydrogen atom (Lipid14 atom type hB) were scaled until satisfactory agreement with experiment was found for ρ and ΔH_{vap} of *cis*-2-hexene, *cis*-5-decene, and *cis*-7-pentadecene. Reducing both the van der Waals radius (R) from 1.459 to 1.25 and the well-depth (ε) from 0.015 to 0.007 resulted in far better agreement for the density values (ρ); however, it proved difficult to correct the heat of vaporization (ΔH_{vap}) of *cis*-5-decene to that of the experimental value by only modifying the LJ parameters. This is due to the high charge on the double bond atoms. A similar problem has previously been encountered by Chiu et al.[13] and Jämbeck et al.[10]

The uncorrected diffusion D_{PBC} was calculated for each alkane using the slope of a mean-square displacement (MSD)
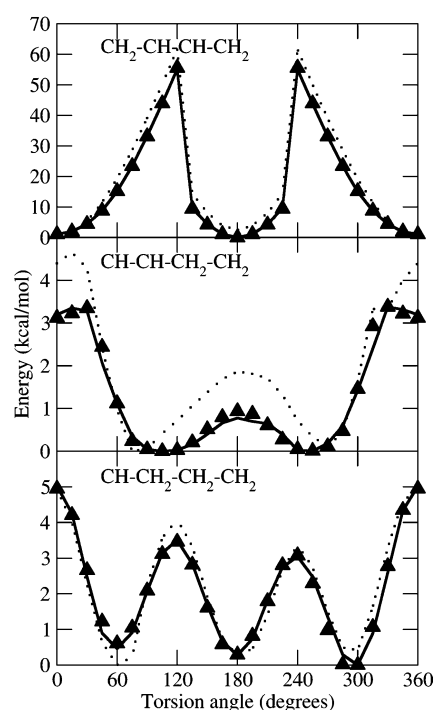
Figure 2. The energy profile for rotating about selected torsions of a *cis*-5-decene molecule. Energy evaluated using QM and the HM-IE method (filled triangle ▲), AMBER with standard GAFF parameters (dotted line), and AMBER with Lipid14 parameters (black line). Torsion fits from the top are as follows: CH₂−CH−CH−CH₂, CH−CH−CH₂−CH₂, and CH−CH₂−CH₂−CH₂.

plot versus time for the centers of mass, averaged over the trajectories of each molecule via the Einstein relation

$$D_{\text{PBC}} = \lim_{t \to \infty} \frac{\langle \Delta r(t)^2 \rangle}{2n_f t} \quad (2)$$

where n_f is the number of dimensions (in this instance $n_f = 3$), and $\Delta r(t)^2$ is the distance that the molecule travels in time t. It is then possible to correct for the system size dependence of a diffusion coefficient calculated under periodic boundaries (D_{PBC}) to yield the corrected diffusion coefficient D_{corr} by adding the correction term derived by Yeh and Hummer[38]

$$D_{\text{corr}} = D_{\text{PBC}} + \frac{k_B T \varepsilon}{2n_f \pi \eta L} \quad (3)$$

where k_B is Boltzmann's constant, T is the temperature, $\varepsilon = 2.837297$, η is the viscosity, and L is the length of the simulation box.

The diffusion was calculated from 100 ns NVE ensemble simulations (extended from the 50 ns NPT runs). PME was used, along with a 10 Å cutoff, at a temperature of 298.15 K. In order to avoid energy and temperature drift, it was necessary to remove the center of mass motion every 500 steps (nscm = 500), make both the shake tolerance and Ewald direct sum tolerance more stringent, and reduce the time step to 1 fs. Diffusion values were then calculated by taking the slope of the linear 2−5 ns region of the MSD versus time curve and the correction calculated using experimental viscosity values. Diffusion results are reported with standard deviations calculated by block averaging, with each 100 ns run divided into five 20 ns blocks.

The *trans*, *gauche*, end *gauche*, double *gauche*, and kinked *gtg′+gtg* conformer populations were evaluated from the 50 ns NPT runs by classifying torsion angles as either *gauche* plus (*g*+) 0−120°, *trans* (*t*) 120−240°, or *gauche* minus (*g*−) 240−360°.

¹³C NMR T_1 relaxation times were calculated from the NPT alkane simulations using the following formula for dipolar relaxation from the reorientation correlation functions of the CH vectors:[39]

$$\frac{1}{NT_1} = (1.855 \times 10^{10}\text{s}^{-2}) \int_0^\infty \langle P_2(\hat{\mu}(0)\hat{\mu}(t)) \rangle \text{d}t \quad (4)$$

This assumes motional narrowing and an effective C−H bond length of 1.117 Å,[40] with N specifying the number of protons bonded to the carbon and $\hat{\mu}$ the CH vector. T_1 relaxation times were calculated from simulations of alkanes of four different chain lengths. These simulations were repeated using the same NPT alkane protocol at the experimentally relevant temperature of 312 K and production runs extended to 200 ns to improve sampling.

Head Group Parameters. It was found that the heat of vaporization of methyl acetate, a model compound representing the ester linkage region connecting the lipid head and tail groups, was not sufficiently close to experiment using GAFF/Lipid11 parameters. In order to correct for this discrepancy with experiment, the Lennard-Jones well-depths of the carbonyl oxygen (oC), carbonyl carbon (cC), and ester oxygen (oS) atoms were scaled until better agreement with experiment was obtained (see Table 2). The ester oxygen parameters were also applied to oxygen atoms in the phosphate region.

The density and heat of vaporization of methyl acetate were calculated using an identical procedure as for the hydrocarbon

Table 2. Thermodynamic Properties of Methyl Acetate Simulated with GAFF/Lipid11 and Lipid14 and Comparison to Experiment[a]

		LJ parameters			
	atom type	radius R (Å)	well-depth ε (kcal mol⁻¹)	ΔH_{vap} (kJ mol⁻¹)	ρ (kg m⁻³)
Lipid11	oC	1.6612	0.210	39.11 ± 0.04	928.38 ± 0.09
	oS	1.6837	0.170		
	cC	1.9080	0.086		
Lipid14	oC	1.6500	0.140	33.0 ± 0.07	925.8 ± 0.05
	oS	1.6500	0.120		
	cC	1.9080	0.070		
Expt				32.29[41]	934.2[41]

[a]All values at 298.15 K.

chains, with a box of 288 methyl acetate molecules applied for the liquid phase calculation. Simulations were run for 60 ns and the final 50 ns used for sampling. Results are reported as block averages (five blocks of 10 ns).

Partial Charges. RESP fitting was performed in exactly the same manner to Lipid11,[22] using the capping groups shown in Figure 3. However a greater number of conformations were used to calculate the average charges for each unit.
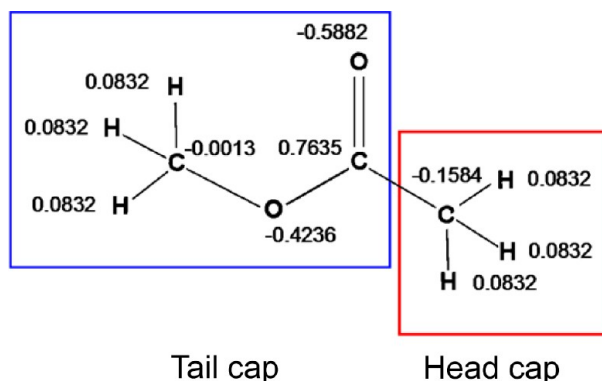
Figure 3. Structure and charges of Lipid11/Lipid14 headgroup and tail group caps.[22]

Twenty-five phosphatidylcholine (PC) and twenty-five phosphatidylethanolamine (PE) head groups were extracted from previous bilayer simulations of DOPC and POPE; while fifty lauroyl (LA), myristoyl (MY), palmitoyl (PA), and oleoyl (OL) tails were extracted from bilayer simulations of DLPC, DMPC, DPPC, and DOPC, respectively. Each headgroup was then capped with a methyl group and each tail capped with an acetate moiety (Figure 3), according to the Lipid11 charge derivation methodology.[22] For each conformation, the ESP was calculated directly from each structure at the HF/6-31G* level using Gaussian 09.[42] Charges were taken as an average over all conformations for each residue. Resulting charges for the PC and PE headgroup residues and the LA, MY, PA, and OL tail group residues are detailed in the Supporting Information.

Head Group Torsion Fits. Two torsions involving the ester linkage region (see Figure 4) were fitted to QM data. The
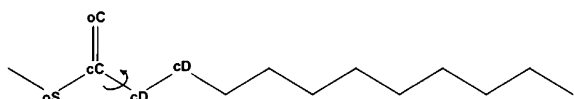
Figure 4. A capped lauroyl tail group residue was used to fit the oS-cC-cD-cD and oC-cC-cD-cD torsions.

scans were performed on a capped lauroyl (LA) tail residue, at 15° increments using the HM-IE method with Gaussian 09.[42] These were then fitted using Paramfit[17,29] for periodicity $n = 1$ to $n = 5$ using the genetic algorithm implemented in Paramfit.

As can be seen from Figure 5 Paramfit brings the oS-cC-cD-cD and oC-cC-cD-cD torsions into substantially better agreement with the QM data.

■ PARAMETERIZATION

Hydrocarbon Parameters. The results for the alkane properties calculated using the updated torsion and LJ parameters are shown in Table 3. The heat of vaporization values increase with alkane chain length, following the
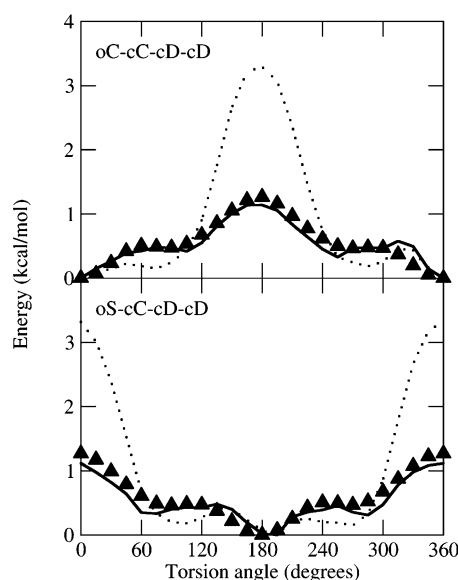
Figure 5. The energy profiles for rotating about selected torsions of a capped lauroyl tail group residue. Energy evaluated using QM and the HM-IE method (filled triangle ▲), AMBER with standard GAFF/Lipid11 parameters (dotted line), and AMBER with Lipid14 parameters (black line). Torsion fits from the top are oC-cC-cD-cD and oS-cC-cD-cD.

experimental trend and converging with experiment as the number of carbon atoms in the chain increases. The simulation values match experiment with an RMS error of 7.67%. The simulated densities are reproduced somewhat better than ΔH_{vap}, with an RMS error of 2.60% when compared to experiment. The diffusion values lie close to experiment and decrease with increasing chain length, following the experimental trend; however, the RMS error between simulation and experiment remains significant at 20.92%. As is also the case with the heat of vaporization results, the main source of this discrepancy is the result for the shorter alkane chains. The better agreement with experiment of these parameters at modeling longer hydrocarbon chains may arise from the use of a high number of octane structures during torsion fitting. Furthermore, this parameter set is intended for the simulation of membrane lipids, which typically contain aliphatic tails that are ten carbon atoms or greater in length.

Thermodynamic properties for a selection of alkenes calculated using the updated LJ and torsion parameters are shown in Table 4. As previously stated, properties of unsaturated chains are not as well reproduced as for alkanes due to the difficulty in tuning LJ parameters to achieve the experimental heat of vaporization, resulting in an RMS error of 13.80% for ΔH_{vap} when compared to experiment. The density values are again better reproduced with an RMS error of 2.35%.

The fractions of *trans*, *gauche*, end *gauche*, double *gauche*, and kinked *gtg'+gtg* conformers per molecule were computed for the selection of alkanes under study (see Table 5). Experimental data, estimated by FTIR, exists only for tridecane;[46] however, the updated Lipid14 parameters reproduce these results extremely well with an overestimation of the end *gauche* and double *gauche* conformations only. Furthermore, the population of gauche conformations per molecule falls close to the experimental value of 35% for all chains investigated (*t/g* ratio ~1.86), meaning that the

Table 3. Thermodynamic and Dynamic Properties of a Selection of Alkane Chains Simulated Using the Updated Lipid14 Parameters and Comparison to Experiment[a]

	ΔH_{vap} (kJ mol^{-1})	ρ (kg m^{-3})	D_{PBC} (10^{-5} cm^2 s^{-1})	D_{corr} (10^{-5} cm^2 s^{-1})
Pentane				
Lipid14	23.03 ± 0.16	592.45 ± 0.16	6.45 ± 0.56	7.1 ± 0.56
Expt	26.43[41]	626.2[41]		5.45[43]
Hexane				
Lipid14	28.54 ± 0.1	636.3 ± 0.09	4.55 ± 0.29	5.02 ± 0.29
Expt	31.56[41]	656,[44] 660.6[41]		4.21[43]
Heptane				
Lipid14	33.37 ± 0.11	667.31 ± 0.14	3.47 ± 0.23	3.85 ± 0.23
Expt	36.57[41]	679.5[41]		3.12[43]
Octane				
Lipid14	38.67 ± 0.31	690.96 ± 0.10	2.11 ± 0.15	2.46 ± 0.15
Expt	41.49[41]	698.6[41]		2.354[45]
Decane				
Lipid14	49.34 ± 0.30	724.47 ± 0.07	1.44 ± 0.15	1.65 ± 0.15
Expt	51.42[41]	726.6[41]		1.39[45]
Tridecane				
Lipid14	64.62 ± 0.27	756.19 ± 0.24	0.48 ± 0.04	0.57 ± 0.04
Expt	66.68[41]	756.4[41]		0.712[45]
Pentadecane				
Lipid14	74.99 ± 0.39	770.67 ± 0.25	0.30 ± 0.02	0.36 ± 0.02
Expt	76.77[41]	768.5[41]		0.461[45]

[a]All values at 298.15 K.

Table 4. Thermodynamic Properties of a Selection of Alkene Chains Simulated Using the Updated Lipid14 Parameters and, Where Available, Comparison to Experiment

	ΔH_{vap} (kJ mol^{-1})	ρ (kg m^{-3})
cis-2-Hexene		
Lipid14	26.17 ± 0.21	656.23 ± 0.13
Expt	32.19[41]	683[44]
cis-5-Decene		
Lipid14	45.27 ± 0.22	739.19 ± 0.16
Expt	42.9[41]	744.5[41]
cis-7-Pentadecene		
Lipid14	69.5 ± 0.22	781.44 ± 0.24
Expt		775[44]

Table 5. Average Number of trans, gauche, End gauche (eg), Double gauche (gg), and gtg'+gtg Conformers Per Alkane Molecule and Comparison to Experiment

	trans	gauche	t/g ratio	eg	gg	gtg'+gtg
Pentane						
Lipid14	1.20	0.80	1.49	0.80	0.13	-
Hexane						
Lipid14	1.83	1.17	1.57	0.83	0.22	0.14
Heptane						
Lipid14	2.49	1.51	1.65	0.83	0.31	0.24
Octane						
Lipid14	3.15	1.85	1.71	0.81	0.39	0.33
Decane						
Lipid14	4.47	2.53	1.77	0.81	0.57	0.54
Tridecane						
Lipid14	6.47	3.53	1.84	0.81	0.82	0.83
Expt[46]	6.5	3.5	1.86	0.68	0.64	0.77
Pentadecane						
Lipid14	7.80	4.20	1.86	0.81	1.00	1.02

overpopulation of *trans* conformations which drives GAFF bilayer simulations into the gel phase is avoided.

The quality of the hydrocarbon parameters was further assessed by calculating the ^{13}C NMR T_1 relaxation times for heptane, decane, tridecane, and pentadecane. Similar to diffusion, this is a dynamic property; however, it depends on the rotation of the CH vector. Results are shown in Figure 6. In
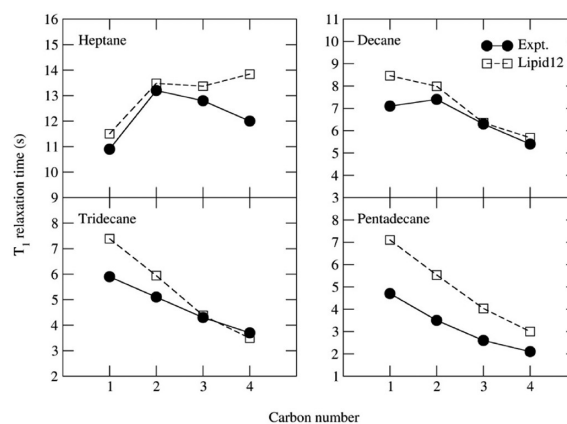
Figure 6. Calculated ^{13}C NMR T_1 relaxation times for selected alkane chains and comparison to experiment.[47] Values at 312 K.

general the simulation values follow the same profile as the experimental data. Simulation values tend to converge with experiment upon moving further from the end carbon of the alkane chains. Although the result for pentadecane is slightly high, the overall comparison between simulation and experiment is reasonable.

LIPID BILAYER SIMULATION

Initial Structures. Bilayers were constructed using the CHARMM Membrane Builder GUI[48] at the relevant

experimental hydration level (see Table 6) and converted to Lipid14 PDB format using the charmmlipid2amber.x script.[17]

Table 6. System Size, Hydration, Temperature, and Simulation Time for the Lipid Bilayer Systems

	no. of lipids	simulation time (ns)	temp (K)	waters/lipid n_W
DLPC	128	5 × 125	303	31.3
DMPC	128	5 × 125	303	25.6
DPPC	128	5 × 125	323	30.1
DOPC	128	5 × 125	303	32.8
POPC	128	5 × 125	303	31
POPE	128	5 × 125	310	32

All systems used the TIP3P water model[49] and had 0.15 M KCl salt concentration added to the water layer, modeled using suitable AMBER parameters.[50]

Equilibration Procedure. The full system was minimized for 10000 steps, of which the first 5000 steps used the steepest descent method and the remaining steps used the conjugate gradient method.[51]

The system was then heated from 0 K to 100 K using Langevin dynamics[52] for 5 ps at constant volume, with weak restraints on the lipid (force constant 10 kcal mol^{-1} Å^{-2}).

Following this, the volume was allowed to change freely and the temperature increased to a lipid dependent value (see Table 6) with a Langevin collision frequency of γ = 1.0 ps^{-1}, and anisotropic Berendsen regulation[37] (1 atm) with a time constant of 2 ps for 100 ps. The same weak restraint of 10 kcal mol^{-1} Å^{-2} was maintained on the lipid molecules.

Production Runs. Constant pressure and constant temperature (NPT) runs were performed on the six bilayers using the AMBER 12 package.[17] The GPU implementation of the AMBER 12 code (bugfix 21) was used to run the simulations on NVIDIA GPU cards, achieving approximately 30 ns per day for the 128-lipid bilayer systems.[17,19] Three dimensional

periodic boundary conditions with the usual minimum image convention were employed. Bonds involving hydrogen were constrained using the SHAKE algorithm,[36] allowing a 2 fs time step. Structural data was recorded every 10 ps. PME was used to treat all electrostatic interactions with a real space cutoff of 10 Å. A long-range analytical dispersion correction was applied to the energy and pressure. All simulations were performed at constant pressure of 1 atm and constant target temperature (Table 6). Temperature was controlled by the Langevin thermostat,[52] with a collision frequency of γ = 1.0 ps^{-1}, as this method was identified as the most suitable in previous work.[25] Pressure was regulated by the anisotropic Berendsen method[37] (1 atm) with a pressure relaxation time of 1.0 ps.

Each lipid type was simulated for 125 ns with five repeats. The first 25 ns of each run was removed for equilibration, resulting in a total of 500 ns of data per lipid system, an aggregate of 3 μs of data. Results are presented as block averages over the five repeats ± standard deviation. The majority of analysis in this paper used PTRAJ or CPPTRAJ analysis routines.[17,53]

To check stability over time of the lipid bilayer systems, the simulations were extended from 125 ns to 250 ns. Additional GPU and CPU validations were also performed, and in all cases the GPU results were consistent with CPU results (see the Supporting Information).

■ VALIDATION

Bilayer Structural Properties. Despite the degree of uncertainty in obtaining accurate experimental values,[72] the bilayer surface area each lipid occupies, or area per lipid, is easily calculated from membrane simulations and gives a quick indication of whether a bilayer is in the correct phase at a given temperature. The area per lipid for each system was calculated using the dimensions of the simulation box as per previous work.[22,26] The A_L for each lipid type is reported in Table 7, with all simulation values within 3% of experimental values,

Table 7. Average Structural Properties over Five Repeats of the Six Lipid Systems Simulated with Lipid14 and Comparison to Experiment

lipid system	area per lipid A_L (Å^2)	volume per lipid V_L (Å^3)	isothermal area compressibility modulus K_A (mNm^{-1})	bilayer thickness D_{HH} (Å)	bilayer Luzzati thickness D_B (Å)	$\Delta D_{B^-H} = (D_B - D_{HH})/2$ (Å)	ratio r of terminal methyl to methylene volume
DLPC							
Lipid14	63.0 ± 0.2	948.9 ± 0.3	281 ± 37	30.4 ± 0.4	30.2 ± 0.1	−0.1 ± 0.2	1.9
Expt	63.2,[54] 60.8[55]	991[54]	-	30.8[54]	31.4[54]	0.8[56]	1.8−2.1[57]
DMPC							
Lipid14	59.7 ± 0.7	1050.2 ± 1.5	264 ± 90	34.7 ± 0.6	35.2 ± 0.4	0.3 ± 0.2	2.2
Expt	60.6,[54] 59.9[55]	1101[4,54]	234[58]	34.4,[59] 35.3[60]	36.3,[54] 36.7,[55] 36.9[59]	0.8[56]	1.8−2.1[57]
DPPC							
Lipid14	62.0 ± 0.3	1177.3 ± 0.5	244 ± 50	37.9 ± 0.5	38.0 ± 0.2	0.1 ± 0.2	2.1
Expt	63.1,[55] 64.3[61]	1232[4]	231[4]	38,[62] 38.3[4]	39.0[55,62]	0.8[56]	1.8−2.1[57]
DOPC							
Lipid14	69.0 ± 0.3	1249.6 ± 0.2	338 ± 31	37.0 ± 0.2	36.2 ± 0.2	−0.4 ± 0.1	2.1
Expt	67.4,[62] 72.5[4]	1303[4]	265,[58] 300,[63] 318[64]	35.3,[65] 36.7,[62,66] 36.9,[4] 37.1[67]	35.9,[4] 36.1,[65,67] 38.7[62]	1.0−1.7[57]	1.8−2.1[57]
POPC							
Lipid14	65.6 ± 0.5	1205.4 ± 0.4	257 ± 47	36.9 ± 0.6	36.8 ± 0.3	−0.1 ± 0.2	1.9
Expt	64.3,[55] 68.3[68]	1256[68]	180−330[69]	37[68]	36.8,[68] 39.1[55]	0.8[56]	1.8−2.1[57]
POPE							
Lipid14	55.5 ± 0.2	1138.7 ± 0.3	350 ± 81	42.4 ± 0.2	41.0 ± 0.1	−0.7 ± 0.1	2.0
Expt	56.6,[70] 59−60[71]	1180[71]	233[70]	39.5[71]	-	-	1.8−2.1[57]
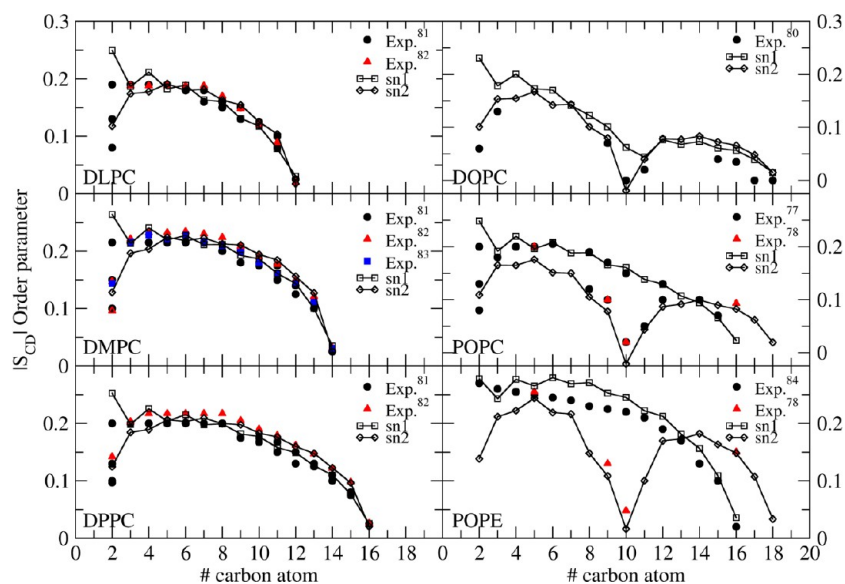
Figure 7. Simulation NMR order parameters for the six lipid systems and comparison to experiment.[77,78,80−84]

indicating that all the bilayers are in the correct L_α-phase. The result for POPE is closer to the older experimental A_L value of 56.6 Å² than the more recent A_L value 59−60 Å². Nevertheless, the A_L should be but one of a number of properties calculated to validate a lipid force field.[73,74]

Experimentally, the volume per lipid V_L is more accurately measured and is thus a better comparison for simulation results than A_L. The volume per lipid was calculated using the dimensions of the simulation box[26] and the volume of a water molecule as determined by simulating 1936 TIP3P waters in the NPT ensemble for 50 ns using an identical procedure to the bilayer simulations at the relevant temperature.

V_L values for each lipid are reported in Table 7, which although systematically underestimated, are within 5% of experimental values. It is likely that the headgroup LJ parameters could be further tuned to remedy this discrepancy, as the thorough reparamaterization of the hydrocarbon chains makes it unlikely that the tail groups are causing this lack of agreement.

This intuition is confirmed when studying the lipid component volumes calculated with the SIMtoEXP software.[75] The headgroup volume of DOPC was found to be 305.41 Å³, which is below the experimental estimate of 319−331 Å³, while the hydrocarbon chain volume of 965.88 Å³ is closer to the experimental range of 972−984 Å³.[57]

The volume breakdown provided by SIMtoEXP was used to calculate the ratio r of terminal methyl to methylene volume. All lipid systems report a value of $r = 1.85−2.17$, within or very close to the experimental range of 1.8−2.1.

Isothermal area compressibility modulus, K_A, was calculated from the fluctuation in the area per lipid.[26] In general, K_A values fall close to experiment, with experimental values falling within the standard deviation of DMPC, DPPC, DOPC and POPC simulation results; however the POPE value comes out high and there is a large standard deviation in all values. Although the DOPC value is above the published experimental value of 300 mN m⁻¹,[63] a personal communication with E. Evans revealed that this K_A value has recently been revised upward to 318 mN m⁻¹,[64] closer to the Lipid14 simulation result. This was not known prior to the lipid simulations.

In this work, the Berendsen method was used for pressure coupling, given that it is the only barostat currently available in the AMBER MD package. It has recently been shown that Berendsen pressure control is not ideal for simulations in which volume fluctuations are important,[76] thus by implementing other barostats into AMBER better K_A results may potentially be achieved. This is a work in progress, the results of which will be shown elsewhere. Furthermore, larger system sizes and longer simulation times could also be investigated, as such changes have been shown to speed up the convergence of K_A values.[74]

The membrane thickness was examined by calculating D_{HH}, the peak-to-peak distance, from electron density profiles of the membranes. Again, satisfactory agreement with experiment is achieved for all lipids, though the POPE value is a little high, indicating that this system is slightly too ordered.

An alternative bilayer thickness, the Luzzati thickness D_B, was calculated using the z-dimension of the simulation box and the integral of the probability distribution of the water density along the z-axis.[9,10] D_B values are found to lie close to experimental values, though the D_B thicknesses for the saturated lipids are slightly underestimated. Given that D_B is the distance between the points along the membrane normal at which the water density is half of its bulk value, this suggests that water is penetrating slightly too far into the hydrophobic region of the bilayer, thereby lowering the value of D_B.

Ordering and Conformation of Lipid Acyl Chains. The ordering of the lipid acyl chains may be determined by calculation of the order parameter S_{CD}. This quantity can be directly compared to experimental S_{CD} values determined by ²H NMR or ¹H−¹³C NMR.[77−80] S_{CD} is a measure of the relative orientation of the C−D bonds with respect to the bilayer normal and was calculated according to

$$S_{CD} = \frac{1}{2}\langle 3\cos^2\theta - 1\rangle \tag{5}$$

where θ is the angle between the bilayer normal and the vector joining C_i to its deuterium atom, and < > represents an ensemble average.

Figure 7 shows the Lipid14 order parameters with comparison to experiment. All lipid systems follow the

Table 8. Analysis of Rotamers and Rotamer Sequences in the Acyl Chains of the Six Lipid Systems − End *gauche* (*eg*), Double *gauche* (*gg*), Kinks (*gtg′*), *gtg′*+*gtg*, and Number of *gauche* (*ng*)

lipid system	eg	gg	gtg′	gtg′+gtg	ng
DLPC					
Lipid14	0.35	0.44	0.28	0.52	2.50
Expt[93]	0.45	0.32	0.88*	-	2.85
DMPC					
Lipid14	0.34	0.48	0.35	0.62	2.82
Expt[94]	0.38	0.67	-	0.44	2.6
DPPC					
Lipid14	0.36	0.66	0.47	0.83	3.58
Expt	0.38,[94] 0.4,[88] 0.54[93]	0.4,[88,93] 0.57[94]	1.19[93a]	0.46,[94] 1.0[88]	2.44,[94] 3.6−4.2,[95] 3.7,[93] 3.8[82]
DOPC					
Lipid14	0.36	0.75	0.37	0.70	3.93
POPC					
Lipid14	0.36	0.69	0.41	0.75	3.73
POPE					
Lipid14	0.35	0.60	0.42	0.73	3.50
Expt[88]	0.05	0.2	-	0.8	-

[a]The *gtg′* sequence may be ascribed to a *gtg′*+*gtg* sequence.[90]
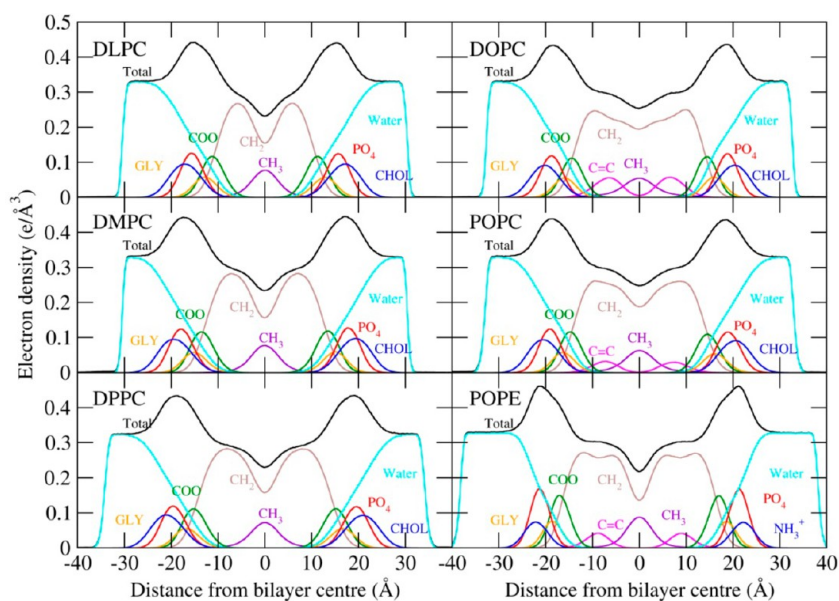
Figure 8. The total and decomposed electron density profiles for each of the six lipid bilayer systems with contributions from water, choline (CHOL), phosphate (PO₄), glycerol (GLY), carbonyl (COO), methylene (CH₂), unsaturated CH═CH and terminal methyls (CH₃).

experimental order parameter trend. The carbon-2 atom of the sn-1 and sn-2 chains display markedly different order parameters owing to the different alignment of the acyl chains in this region. Experimentally, it has been found that the S_{CD} order parameter of the C-D bonds near the headgroup in the sn-1 chains are greater than the sn-2 chains.[85,86] Splitting of the order parameter value of the sn-2 chain from the sn-1 chain is observed for the simulated lipid systems. The unsaturated chain of the DOPC, POPC and POPE lipids show a distinctive drop at the carbon-9 and -10 positions due to the *cis* double bond. The S_{CD} values for the sn-1 chain of POPE are a little high, indicating that POPE may be slightly too ordered. In agreement with Jämbeck et al., the two chains of DOPC show differing behavior, the sn-1 chain having higher S_{CD} values about the double bond than the sn-2 chain.[87]

The conformation of the acyl chains may be examined by analyzing the rotamers and rotamer sequences along the lipid

tails and comparing results to experimental data collected by Fourier transform infrared (FTIR) spectroscopy.[88] FTIR can determine the number of *trans* (*t*) and *gauche* (*g*) conformers and sequences of *t* and *g* (end *gauche eg*, double *gauche gg*, *gtg*, and kinks *gtg′*). The lipid bilayer simulations were analyzed by denoting torsion angles φ in the acyl chains as either *t* ($\varphi < -150°$ or $\varphi > 150°$), g- ($-90° \leq \varphi < -30°$) or g+ ($30° < \varphi \leq 90°$).[89] The rotamer sequence *gtg* correspond to g+tg+ or g-tg- while the sequence (or kinks) *gtg′* corresponds to g+tg- or g-tg+.

Results are shown in Table 8 and are in general satisfactorily close to available experimental values. The discrepancies observed between simulation and experimental values of *gtg′* for DLPC and DPPC may result from the experimental ambiguity in assigning *gtg* and *gtg′* wagging modes.[90] These results also confirm that the bilayers are in the correct phase, as the gel-to-liquid phase transition is associated with an increase
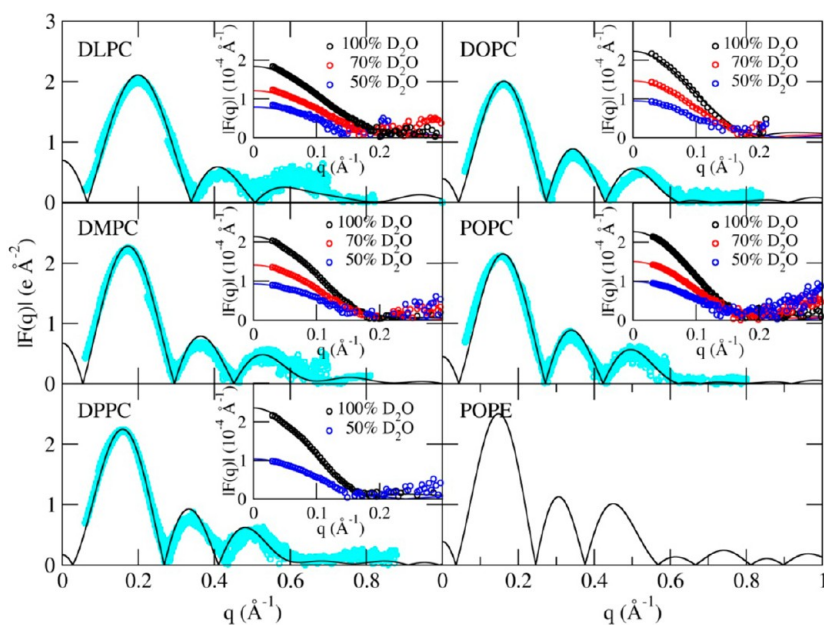
Figure 9. Simulation X-ray scattering form factors for the six lipid systems (black line) and comparison to experiment[54,55,62,66,68] (cyan circles). Inset: Simulation neutron scattering form factors at 100% D_2O (black line), 70% D_2O (red line), and 50% D_2O (blue line) and comparison to experiment[55,96] (black, red, and blue circles, respectively).

in the number of *gauche* rotamers and kink rotamer sequences.[90−92] However the *eg* and *gg* results for POPE are not in accordance with the experimental values obtained by Senak et al. using FTIR,[88] who found a marked increase in *eg*, *gg*, and *gtg′+gtg* values going from DPPE to DPPC because of the tighter packing of the PE lipid in the L_α phase. The present simulation values for POPE and POPC, though, are similar.

Electron Density Profiles. The electron density profiles (EDP) were calculated by assuming an electron charge equal to the atomic number minus the atomic partial charge, located at the center of each atom. Profiles have also been decomposed into contributions from the following groups: water, choline (CHOL), phosphate (PO_4), glycerol (GLY), carbonyl (COO), methylene (CH_2), unsaturated CH=CH and terminal methyls (CH_3). These profiles, shown in Figure 8, are all symmetrical, with water penetrating up to the carbonyl groups, leaving the terminal methyl groups dehydrated in agreement with experimental findings.[54,68,61] The electron density profiles were then utilized for the calculation of scattering form factors using the SIMtoEXP software.[75]

Scattering Form Factors. Scattering data allow direct comparison between lipid bilayer simulation and experiment, avoiding any intermediate modeling of experimental raw data.[57] X-ray and neutron scattering form factors can be computed by Fourier transformation of simulation electron density profiles and compared to experimental scattering data.

Recent work determined the areas per lipid (A_X and A_N) at which DOPC bilayer simulations best replicate the experimental X-ray scattering and neutron scattering data by varying the area per lipid through application of a surface tension, with the ideal situation being $A_X = A_N = A_{NPT}$ (bilayer is run in the tensionless NPT ensemble).[57] In this work we were concerned with validating the Lipid14 parameters for tensionless bilayer simulation only; thus we report the X-ray and neutron scattering form factors for A_{NPT} only.

It can be seen from Figure 9 that there is general agreement between both the X-ray and neutron scattering form factors for

all lipids for which there is experimental scattering data available, indicating that the simulated bilayers have the correct structure. In general the minima of the experimental F(q) profiles are correctly reproduced, as are the relative lobe heights.

The quantity $\Delta D_{B\text{-}H}$ was computed from the membrane thickness values (see Table 7). Agreement with X-ray scattering data is sensitive to the value of D_{HH}, while agreement with neutron scattering data is sensitive to the value of D_B. Therefore it has been proposed that bilayer simulations should aim to replicate experimental $\Delta D_{B\text{-}H}$ values to best achieve agreement with both types of scattering data, where $\Delta D_{B\text{-}H} = (D_B\text{-}D_{HH})/2$.[57] The GROMOS united-atom lipid force field has been shown to match experiment for simulation $\Delta D_{B\text{-}H}$ results.[56,57] As evidenced by Table 7, Lipid14 $\Delta D_{B\text{-}H}$ values are lower than those found by experiment, though all simulation values do maintain a large standard deviation. In fact, analysis of $\Delta D_{B\text{-}H}$ results for two other all-atom lipid force fields, CHARMM36[8] and Slipids[10,87] indicates that this quantity is difficult to reproduce using all-atom models, with only the Slipids POPC result falling close to experiment. Figure 10 plots $\Delta D_{B\text{-}H}$ values against area per lipid for CHARMM36,[56] Slipids,[10,87] and AMBER Lipid14, displaying a downward trend in $\Delta D_{B\text{-}H}$ with increasing area per lipid, in disagreement with the experimental trend. Results for Lipid14 are similar to CHARMM36 and most Slipids values. Improving this discrepancy with experiment for Lipid14 may further improve the comparison with scattering data; however, present simulation scattering profiles are still seen to be in satisfactory agreement with experiment.

Lipid Lateral Diffusion. To assess the ability of the Lipid14 parameters to reproduce dynamic lipid properties, the lipid lateral diffusion coefficient D_{xy} was calculated using the Einstein relation (eq 2) with two degrees of freedom ($n_f = 2$). Diffusion coefficients were computed for each lipid as a block average over the five NPT production runs. The mean-square-displacement (MSD) curves were determined using window lengths spanning 20 ns and averaged over different time origins
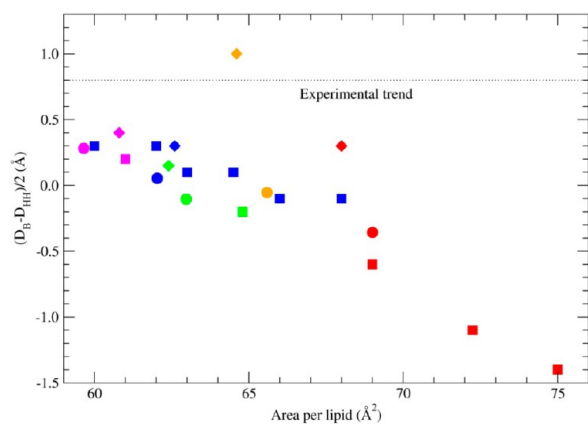
Figure 10. Plot of $\Delta D_{B\text{-}H}$ versus area per lipid A_L for the three all-atom lipid force fields CHARMM36 (squares), Slipids (diamonds), and AMBER Lipid14 (circles). Values shown for DLPC (green), DMPC (magenta), DPPC (blue), DOPC (red), and POPC (orange).

Figure 11. Time averaged mean square displacement of the center of mass of the lipid molecules versus NVE simulation time.

separated by 200 ps. The slope of this curve yields the diffusion coefficient using eq 2, with the linear 10−20 ns region used to perform the fit. Prior to the MSD calculation, the lipid coordinates were corrected to remove the artificial center of mass drift of each monolayer.[73]

Results are of the same order of magnitude as experimental values; although in general they are underestimated. Unlike the bulk alkane work there is no correction term to account for collective motion which cannot be sampled using a periodic box of limited size. Accordingly, the underestimation may be a result of size effects. As highlighted by Poger et al. there is a widespread in experimental lipid lateral diffusion values in the literature, with a range of experimental techniques applied to the calculation of diffusion values.[105] Even different groups applying the same experimental technique do not necessarily yield comparable diffusion coefficients. Our calculated diffusion coefficients are nonetheless found to be in good agreement with other simulation values.[10,23,87,105−107]

Given that the production runs were performed in the NPT ensemble and that temperature regulation methods such as Langevin dynamics, which randomizes particle velocities, may affect dynamic properties such as diffusion, the lipid lateral diffusion was also determined in the microcanonical (NVE) ensemble. A single production run of each lipid system was extended into the NVE ensemble for 100 ns using the same simulation settings as used for the alkane diffusion runs (see Parameterization Strategy). Resulting time averaged MSD curves are shown in Figure 11, and calculated diffusion coefficients are reported in Table 9. Although similar to the D_{xy} values determined from the NPT runs, the diffusion coefficients from the NVE runs are slightly higher, with the results for DPPC and DOPC showing the largest differences. This supports a recent study on the effect of temperature control on dynamic properties by Basconi et al.,[108] who found that diffusion coefficients calculated from simulations applying Langevin dynamics approach the coefficients derived from NVE simulations, provided weak coupling is used for the temperature regulation.

Lipid lateral diffusion is known to occur via two regimes: fast 'rattling' of the lipid in the local solvation cage[109] and slower, long distance diffusion in the plane of the bilayer. The two regimes are clearly observed in the MSD versus time curves (Figure 11) and are also revealed by computing the diffusion
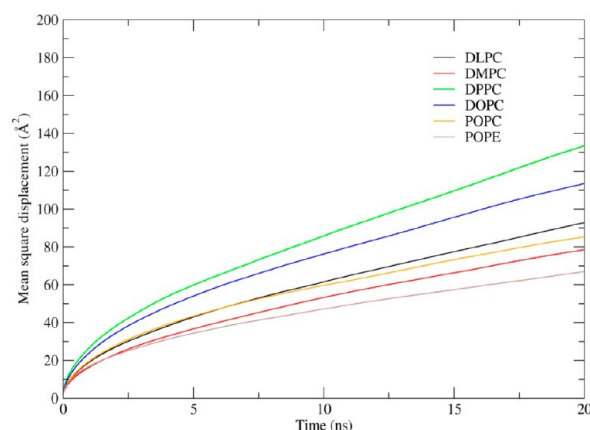
coefficients using different time ranges of the MSD curve. Figure 12 plots the diffusion coefficient D_{xy} against the starting time for fitting the MSD slope. Time windows were either 100 ps long (fit starts between 10 ps and 500 ps) or 500 ps long (fit starts between 500 ps and 20 ns).[23] D_{xy} values decrease smoothly and then converge at a value representing the long time diffusion of lipids in the bilayer plane.

■ CONCLUSIONS

The Lipid14 force field represents a significant advancement for the simulation of phospholipids in the AMBER MD package. Hydrocarbon parameters have been refined, resulting in good reproduction of thermodynamic and dynamic properties for a number of simple carbon chains, thus we can be confident that the hydrocarbon region of the lipid membrane is correctly represented. Head group parameters have also been updated, with the final parameter set finding good agreement with experiment for a range of properties, including the area per lipid, volume per lipid, bilayer thickness, NMR order parameters, scattering data, and lipid lateral diffusion, without applying a surface tension in the simulations. Crucially, the experimental raw data that requires no empirical input to derive, namely the NMR order parameters and scattering data, are well reproduced. Results for POPE however indicate that PE lipids may require further attention, as the order parameter results for POPE indicate that it remains somewhat artificially ordered in comparison to experiment. Results from five GPU repeats and CPU runs are seen to be consistent (these additional results are provided in the Supporting Information), with a number of tests performed on GPUs using both different starting structures and extending production runs to 250 ns. Future improvements may involve further refinement of parameters in order to address the underestimation of the volume per lipid and bilayer Luzzati thickness values in addition to PE lipid types.

Although the present study only concerns the validation of Lipid14 for the simulation of three saturated and three unsaturated lipids, the modular nature of the Lipid14 force field allows for a number of different lipids to be constructed from headgroup and tail group 'building blocks' and for the easy insertion of new lipid species into the force field. The Lipid14 charge derivation follows the usual AMBER convention, making this force field compatible with other AMBER potentials, such as the General Amber Force Field[16] and the ff99SB protein force field.[14] As such, the interaction of other

K

dx.doi.org/10.1021/ct4010307 | J. Chem. Theory Comput. XXXX, XXX, XXX−XXX

Table 9. Lipid Lateral Diffusion Coefficients Calculated from NPT Runs, NVE Runs, and Experimental Values

lipid system	calcd NPT D_{xy} (10^{-8} cm^2 s^{-1})	calcd NVE D_{xy} (10^{-8} cm^2 s^{-1})	simulation temp (K)	exptl D_{xy} (10^{-8} cm^2 s^{-1})	exptl temp (K)
DLPC	7.65	7.78	303	8.5[97]	298
DMPC	5.05	6.32	303	5.95,[98] 9[99,100]	303, 303
DPPC	9.21	11.94	323	12.5,[101] 15.2[102]	323, 323
DOPC	6.48	9.49	303	11.5,[100] 17[103]	303, 308
POPC	5.74	6.54	303	10.7[100]	303
POPE	4.67	4.85	310	5.2[104a]	305

[a]Cell culture membrane containing 78% POPE at 305 K.
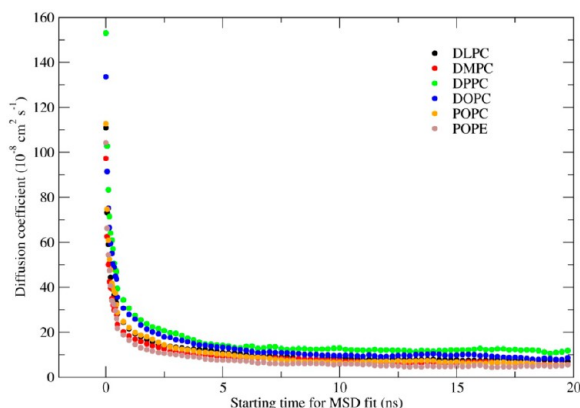
Figure 12. Lateral diffusion coefficients for the six lipid types calculated using different time ranges of the mean square displacement curve for the linear fit.

species, such as small molecules or proteins, with lipid membranes can be studied in AMBER using the Lipid14 force field.

ASSOCIATED CONTENT

Ⓢ Supporting Information

Details of the Lipid14 atom types, partial charges, and force field parameters. Also included are the bilayer results for additional GPU and CPU runs. This material is available free of charge via the Internet at http://pubs.acs.org.

AUTHOR INFORMATION

Corresponding Authors
*E-mail: ross@rosswalker.co.uk.
*E-mail: i.gould@imperial.ac.uk.

Author Contributions
[†]These authors contributed equally.

Notes
The authors declare no competing financial interest.

ACKNOWLEDGMENTS

REFERENCES

(1) van Meer, G.; Voelker, D. R.; Feigenson, G. W. Membrane lipids: where they are and how they behave. *Nat. Rev. Mol. Cell Biol.* **2008**, *9* (2), 112−124.

(2) Lodish, H.; Berk, A.; Kaiser, C. A.; Scott, M. P.; Bretscher, A.; Ploegh, H.; Matsudaira, P. *Molecular Cell Biology*, 6th ed.; W. H. Freeman: New York, 2007.

(3) Phillips, R.; Ursell, T.; Wiggins, P.; Sens, P. Emerging roles for lipids in shaping membrane-protein function. *Nature* **2009**, *459* (7245), 379−385.

(4) Nagle, J. F.; Tristram-Nagle, S. Structure of lipid bilayers. *Biochim. Biophys. Acta* **2000**, *1469* (3), 159−195.

(5) Katsaras, J.; Gutberlet, T. *Lipid bilayers: Structure and interactions*; Springer-Verlag: Berlin, 2001.

(6) Tieleman, D. P.; Marrink, S. J.; Berendsen, H. J. A computer perspective of membranes: molecular dynamics studies of lipid bilayer systems. *Biochim. Biophys. Acta* **1997**, *1331*, 235−270.

(7) Berger, O.; Edholm, O.; Jähnig, F. Molecular dynamics simulations of a fluid bilayer of dipalmitoylphosphatidylcholine at full hydration, constant pressure, and constant temperature. *Biophys. J.* **1997**, *72*, 2002−2013.

(8) Klauda, J. B.; Venable, R. M.; Freites, J. A.; O'Connor, J. W.; Tobias, D. J.; Mondragon-Ramirez, C.; Vorobyov, I.; MacKerell, A. D.; Pastor, R. W. Update of the CHARMM all-atom additive force field for lipids: Validation on Six lipid types. *J. Phys. Chem. B* **2010**, *114* (23), 7830−7843.

(9) Poger, D.; Van Gunsteren, W. F.; Mark, A. E. A new force field for simulating phosphatidylcholine bilayers. *J. Comput. Chem.* **2010**, *31* (6), 1117−1125.

(10) Jämbeck, J. P. M.; Lyubartsev, A. P. Derivation and systematic validation of a refined all-atom force field for phosphatidylcholine lipids. *J. Phys. Chem. B* **2012**, *116* (10), 3164−3179.

(11) Marrink, S. J.; Risselada, H. J.; Yefimov, S.; Tieleman, D. P.; de Vries, A. H. The MARTINI force field: Coarse grained model for biomolecular simulations. *J. Phys. Chem. B* **2007**, *111* (27), 7812−7824.

(12) Orsi, M.; Essex, J. W. The ELBA force field for coarse-grain modeling of lipid membranes. *PLoS One* **2011**, *6* (12), e28637.

(13) Chiu, S.-W.; Pandit, S. A.; Scott, H. L.; Jakobsson, E. An improved united atom force field for simulation of mixed lipid bilayers. *J. Phys. Chem. B* **2009**, *113* (9), 2748−2763.

(14) Hornak, V.; Abel, R.; Okur, A.; Strockbine, B.; Roitberg, A.; Simmerling, C. Comparison of multiple Amber force fields and development of improved protein backbone parameters. *Proteins: Struct., Funct., Bioinf.* **2006**, *65* (3), 712−725.

(15) Kirschner, K. N.; Yongye, A. B.; Tschampel, S. M.; González-Outeiriño, J.; Daniels, C. R.; Foley, B. L.; Woods, R. J. GLYCAM06: A generalizable biomolecular force field. Carbohydrates. *J. Comput. Chem.* **2008**, *29* (4), 622−655.

(16) Wang, J.; Wolf, R. M.; Caldwell, J. W.; Kollman, P. A.; Case, D. A. Development and testing of a general amber force field. *J. Comput. Chem.* **2004**, *25*, 1157−1174.

(17) Case, D. A.; Darden, T. A.; Cheatham, T. E., III; Simmerling, C. L.; Wang, J.; Duke, R. E.; Luo, R.; Walker, R. C.; Zhang, W.; Merz, K. M.; Roberts, B.; Hayik, S.; Roitberg, A.; Seabra, G.; Swails, J.; Goetz, A. W.; Kolossváry, I.; Wong, K. F.; Paesani, F.; Vanicek, J.; Wolf, R. M.; Liu, J.; Wu, X.; Brozell, S. R.; Steinbrecher, T.; Gohlke, H.; Cai, Q.; Ye, X.; Wang, J.; Hsieh, M.-J.; Cui, G.; Roe, D. R.; Mathews, D. H.; Seetin, M. G.; Salomon-Ferrer, R.; Sagui, C.; Babin, V.; Luchko, T.; Gusarov, S.; Kovalenko, A.; Kollman, P. A. *AMBER 12*; University of California: San Francisco, 2012.

(18) Salomon-Ferrer, R.; Case, D. A.; Walker, R. C. An overview of the Amber biomolecular simulation package. *Wiley Interdiscip. Rev.: Comput. Mol. Sci.* **2013**, *3* (2), 198−210.

(19) Götz, A. W.; Williamson, M. J.; Xu, D.; Poole, D.; Le Grand, S.; Walker, R. C. Routine microsecond molecular dynamics simulations with AMBER on GPUs. 1. Generalized Born. *J. Chem. Theory Comput.* **2012**, *8* (5), 1542−1555.

(20) Salomon-Ferrer, R.; Götz, A. W.; Poole, D.; Le Grand, S.; Walker, R. C. Routine microsecond molecular dynamics simulations with Amber on GPUs. 2. Explicit solvent particle mesh Ewald. *J. Chem. Theory Comput.* **2013**, *9* (9), 3878−3888.

(21) Le Grand, S.; Götz, A. W.; Walker, R. C. SPFP: Speed without compromise—A mixed precision model for GPU accelerated molecular dynamics simulations. *Comput. Phys. Commun.* **2013**, *184* (2), 374−380.

(22) Skjevik, Å. A.; Madej, B. D.; Walker, R. C.; Teigen, K. LIPID11: A modular framework for lipid simulations using Amber. *J. Phys. Chem. B* **2012**, *116* (36), 11124−11136.

(23) Siu, S. W.; Vacha, R.; Jungwirth, P.; Bockmann, R. A. Biomolecular simulations of membranes: physical properties from different force fields. *J. Chem. Phys.* **2008**, *128* (12), 125103.

(24) Jójárt, B.; Martinek, T. A. Performance of the general amber force field in modeling aqueous POPC membrane bilayers. *J. Comput. Chem.* **2007**, *28* (12), 2051−2058.

(25) Rosso, L.; Gould, I. R. Structure and dynamics of phospholipid bilayers using recently developed general all-atom force fields. *J. Comput. Chem.* **2008**, *29* (1), 24−37.

(26) Dickson, C. J.; Rosso, L.; Betz, R. M.; Walker, R. C.; Gould, I. R. GAFFlipid: A general Amber force field for the accurate molecular dynamics simulation of phospholipid. *Soft Matter* **2012**, *8*, 9617−9627.

(27) Siu, S. W. I.; Pluhackova, K.; Böckmann, R. A. Optimization of the OPLS-AA force field for long hydrocarbons. *J. Chem. Theory Comput.* **2012**, *8* (4), 1459−1470.

(28) Klauda, J. B.; Brooks, B. R.; MacKerell, A. D.; Venable, R. M.; Pastor, R. W. An ab initio study on the torsional surface of alkanes and its effect on molecular simulations of alkanes and a DPPC bilayer. *J. Phys. Chem. B* **2005**, *109* (11), 5300−5311.

(29) Betz, R. M.; Walker, R. C. Paramfit: Optimization of potential energy function parameters for molecular dynamics. Manuscript in preparation.

(30) Bayly, C. I.; Cieplak, P.; Cornell, W.; Kollman, P. A. A well-behaved electrostatic potential based method using charge restraints for deriving atomic charges: the RESP model. *J. Phys. Chem.* **1993**, *97* (40), 10269−10280.

(31) Sonne, J.; Jensen, M. Ø.; Hansen, F. Y.; Hemmingsen, L.; Peters, G. H. Reparameterization of all-atom dipalmitoylphosphati-

dylcholine lipid parameters enables simulation of fluid bilayers at zero tension. *Biophys. J.* **2007**, *92* (12), 4157−4167.

(32) Klauda, J. B.; Garrison, S. L.; Jiang, J.; Arora, G.; Sandler, S. I. HM-IE: Quantum chemical hybrid methods for calculating interaction energies. *J. Phys. Chem. A* **2003**, *108* (1), 107−112.

(33) Davis, J. E.; Warren, G. L.; Patel, S. Revised charge equilibration potential for liquid alkanes. *J. Phys. Chem. B* **2008**, *112* (28), 8298−8310.

(34) Wang, J.; Hou, T. Application of molecular dynamics simulations in molecular property prediction. 1. density and heat of vaporization. *J. Chem. Theory Comput.* **2011**, *7* (7), 2151−2165.

(35) Darden, T.; York, D.; Pedersen, L. Particle mesh Ewald: An N-log(N) method for Ewald sums in large systems. *J. Chem. Phys.* **1993**, *98* (12), 10089−10092.

(36) Ryckaert, J.-P.; Ciccotti, G.; Berendsen, H. J. C. Numerical integration of the cartesian equations of motion of a system with constraints: molecular dynamics of n-alkanes. *J. Comput. Phys.* **1977**, *23* (3), 327−341.

(37) Berendsen, H. J. C.; Postma, J. P. M.; van Gunsteren, W. F.; DiNola, A.; Haak, J. R. Molecular dynamics with coupling to an external bath. *J. Chem. Phys.* **1984**, *81* (8), 3684−3690.

(38) Yeh, I.-C.; Hummer, G. System-size dependence of diffusion coefficients and viscosities from molecular dynamics simulations with periodic boundary conditions. *J. Phys. Chem. B* **2004**, *108* (40), 15873−15879.

(39) Lipari, G.; Szabo, A. Effect of librational motion on fluorescence depolarization and nuclear magnetic resonance relaxation in macromolecules and membranes. *Biophys. J.* **1980**, *30* (3), 489−506.

(40) Ottiger, M.; Bax, A. Determination of Relative N−HN, N−C′, Cα−C′, and Cα−Hα effective bond lengths in a protein by NMR in a dilute liquid crystalline phase. *J. Am. Chem. Soc.* **1998**, *120* (47), 12334−12341.

(41) Haynes, W. M. *CRC Handbook of Chemistry and Physics*, 93rd ed.; CRC Press: Boca Raton, FL, 2012−2013.

(42) Frisch, M. J.; Trucks, G. W.; Schlegel, H. B.; Scuseria, G. E.; Robb, M. A.; Cheeseman, J. R.; Scalmani, G.; Barone, V.; Mennucci, B.; Petersson, G. A.; Nakatsuji, H.; Caricato, M.; Li, X.; Hratchian, H. P.; Izmaylov, A. F.; Bloino, J.; Zheng, G.; Sonnenberg, J. L.; Hada, M.; Ehara, M.; Toyota, K.; Fukuda, R.; Hasegawa, J.; Ishida, M.; Nakajima, T.; Honda, Y.; Kitao, O.; Nakai, H.; Vreven, T.; Montgomery, J. A., Jr.; Peralta, J. E.; Ogliaro, F.; Bearpark, M.; Heyd, J. J.; Brothers, E.; Kudin, K. N.; Staroverov, V. N.; Kobayashi, R.; Normand, J.; Raghavachari, K.; Rendell, A.; Burant, J. C.; Iyengar, S. S.; Tomasi, J.; Cossi, M.; Rega, N.; Millam, N. J.; Klene, M.; Knox, J. E.; Cross, J. B.; Bakken, V.; Adamo, C.; Jaramillo, J.; Gomperts, R.; Stratmann, R. E.; Yazyev, O.; Austin, A. J.; Cammi, R.; Pomelli, C.; Ochterski, J. W.; Martin, R. L.; Morokuma, K.; Zakrzewski, V. G.; Voth, G. A.; Salvador, P.; Dannenberg, J. J.; Dapprich, S.; Daniels, A. D.; Farkas, Ö.; Foresman, J. B.; Ortiz, J. V.; Cioslowski, J.; Fox, D. J. *Gaussian 09*, Revision A.1; Gaussian Inc.: Wallingford, CT, 2009.

(43) Douglass, D. C.; McCall, D. W. Diffusion in paraffin hydrocarbons. *J. Phys. Chem.* **1958**, *62* (9), 1102−1107.

(44) Yaws, C. L. Yaws' Handbook of Physical Properties for Hydrocarbons and Chemicals. http://www.knovel.com/web/portal/browse/display?_EXT_KNOVEL_DISPLAY_bookid=2147 (accessed February 19, 2013).

(45) Tofts, P. S.; Lloyd, D.; Clark, C. A.; Barker, G. J.; Parker, G. J. M.; McConville, P.; Baldock, C.; Pope, J. M. Test liquids for quantitative MRI measurements of self-diffusion coefficient in vivo. *Magn. Reson. Med.* **2000**, *43* (3), 368−374.

(46) Holler, F.; Callis, J. B. Conformation of the hydrocarbon chains of sodium dodecyl sulfate molecules in micelles: an FTIR study. *J. Phys. Chem.* **1989**, *93* (5), 2053−2058.

(47) Lyerla, J. R.; McIntyre, H. M.; Torchia, D. A. A 13C nuclear magnetic resonance study of alkane motion. *Macromolecules* **1974**, *7* (1), 11−14.

(48) Jo, S.; Lim, J. B.; Klauda, J. B.; Im, W. CHARMM-GUI membrane builder for mixed bilayers and its application to yeast membranes. *Biophys. J.* **2009**, *97* (1), 50−58.

(49) Jorgensen, W. L.; Chandrasekhar, J.; Madura, J. D.; Impey, R. W.; Klein, M. L. Comparison of simple potential functions for simulating liquid water. *J. Chem. Phys.* **1983**, *79* (2), 926−935.

(50) Joung, I. S.; Cheatham, T. E. Determination of alkali and halide monovalent ion parameters for use in explicitly solvated biomolecular simulations. *J. Phys. Chem. B* **2008**, *112* (30), 9020−9041.

(51) Press, W. H.; Teukolsky, S. A.; Vetterling, W. T.; Flannery, B. P. *Numerical Recipes: The Art of Scientific Computing*, 3rd ed. ed.; Cambridge University Press: New York, 2007.

(52) Pastor, R.; Brooks, B.; Szabo, A. An analysis of the accuracy of Langevin and molecular dynamics algorithms. *Mol. Phys.* **1988**, *65* (6), 1409−1419.

(53) Roe, D. R.; Cheatham, T. E. PTRAJ and CPPTRAJ: Software for processing and analysis of molecular dynamics trajectory data. *J. Chem. Theory Comput.* **2013**, *9* (7), 3084−3095.

(54) Kučerka, N.; Liu, Y.; Chu, N.; Petrache, H. I.; Tristram-Nagle, S.; Nagle, J. F. Structure of fully hydrated fluid phase DMPC and DLPC lipid bilayers using X-ray scattering from oriented multilamellar arrays and from unilamellar vesicles. *Biophys. J.* **2005**, *88* (4), 2626−2637.

(55) Kučerka, N.; Nieh, M.-P.; Katsaras, J. Fluid phase lipid areas and bilayer thicknesses of commonly used phosphatidylcholines as a function of temperature. *Biochim. Biophys. Acta* **2011**, *1808* (11), 2761−2771.

(56) Nagle, J. F. Introductory lecture: Basic quantities in model biomembranes. *Faraday Discuss.* **2013**, *161* (0), 11−29.

(57) Braun, A. R.; Sachs, J. N.; Nagle, J. F. Comparing simulations of lipid bilayers to scattering data: The GROMOS 43A1-S3 force field. *J. Phys. Chem. B* **2013**, *117* (17), 5065−5072.

(58) Rawicz, W.; Olbrich, K. C.; McIntosh, T.; Needham, D.; Evans, E. Effect of chain length and unsaturation on elasticity of lipid bilayers. *Biophys. J.* **2000**, *79* (1), 328−339.

(59) Petrache, H. I.; Tristram-Nagle, S.; Nagle, J. F. Fluid phase structure of EPC and DMPC bilayers. *Chem. Phys. Lipids* **1998**, *95* (1), 83−94.

(60) Klauda, J. B.; Kučerka, N.; Brooks, B. R.; Pastor, R. W.; Nagle, J. F. Simulation-based methods for interpreting X-ray data from lipid bilayers. *Biophys. J.* **2006**, *90* (8), 2796−2807.

(61) Kučerka, N.; Tristram-Nagle, S.; Nagle, J. F. Closer look at structure of fully hydrated fluid phase DPPC bilayers. *Biophys. J.* **2006**, *90* (11), L83−L85.

(62) Kučerka, N.; Nagle, J. F.; Sachs, J. N.; Feller, S. E.; Pencer, J.; Jackson, A.; Katsaras, J. Lipid bilayer structure determined by the simultaneous analysis of neutron and X-ray scattering data. *Biophys. J.* **2008**, *95* (5), 2356−2367.

(63) Evans, E.; Rawicz, W.; Smith, B. A. Concluding remarks back to the future: mechanics and thermodynamics of lipid biomembranes. *Faraday Discuss.* **2013**, *161* (0), 591−611.

(64) Evans, E. *Personal Communication - DOPC isothermal compressibility modulus from X-ray data at 293 K*; 2014.

(65) Tristram-Nagle, S.; Petrache, H. I.; Nagle, J. F. Structure and interactions of fully hydrated dioleoylphosphatidylcholine bilayers. *Biophys. J.* **1998**, *75* (2), 917−925.

(66) Pan, J.; Tristram-Nagle, S.; Kučerka, N.; Nagle, J. F. Temperature dependence of structure, bending rigidity, and bilayer interactions of dioleoylphosphatidylcholine bilayers. *Biophys. J.* **2008**, *94* (1), 117−124.

(67) Liu, Y.; Nagle, J. F. Diffuse scattering provides material parameters and electron density profiles of biomembranes. *Phys. Rev. E* **2004**, *69* (4), 040901.

(68) Kučerka, N.; Tristram-Nagle, S.; Nagle, J. F. Structure of fully hydrated fluid phase lipid bilayers with monounsaturated chains. *J. Membr. Biol.* **2006**, *208* (3), 193−202.

(69) Binder, H.; Gawrisch, K. Effect of unsaturated lipid chains on dimensions, molecular order and hydration of membranes. *J. Phys. Chem. B* **2001**, *105* (49), 12378−12390.

(70) Rand, R. P.; Parsegian, V. A. Hydration forces between phospholipid bilayers. *Biochim. Biophys. Acta* **1989**, *988* (3), 351−376.

(71) Rappolt, M.; Hickel, A.; Bringezu, F.; Lohner, K. Mechanism of the lamellar/inverse hexagonal phase transition examined by high resolution X-ray diffraction. *Biophys. J.* **2003**, *84* (5), 3111−3122.

(72) Nagle, J. F.; Tristram-Nagle, S. Lipid bilayer structure. *Curr. Opin. Struct. Biol.* **2000**, *10* (4), 474−480.

(73) Anézo, C.; de Vries, A. H.; Höltje, H.-D.; Tieleman, D. P.; Marrink, S.-J. Methodological issues in lipid bilayer simulations. *J. Phys. Chem. B* **2003**, *107* (35), 9424−9433.

(74) Poger, D.; Mark, A. E. On the validation of molecular dynamics simulations of saturated and cis-monounsaturated phosphatidylcholine lipid bilayers: A comparison with experiment. *J. Chem. Theory Comput.* **2009**, *6* (1), 325−336.

(75) Kučerka, N.; Katsaras, J.; Nagle, J. Comparing membrane simulations to scattering experiments: Introducing the SIMtoEXP software. *J. Membr. Biol.* **2010**, *235* (1), 43−50.

(76) Shirts, M. R. Simple quantitative tests to validate sampling from thermodynamic ensembles. *J. Chem. Theory Comput.* **2012**, *9* (2), 909−926.

(77) Seelig, J.; Waespe-Sarcevic, N. Molecular order in cis and trans unsaturated phospholipid bilayers. *Biochemistry* **1978**, *17* (16), 3310−3315.

(78) Perly, B.; Smith, I. C. P.; Jarrell, H. C. Acyl chain dynamics of phosphatidylethanolamines containing oleic acid and dihydrosterculic acid: deuteron NMR relaxation studies. *Biochemistry* **1985**, *24* (17), 4659−4665.

(79) Lafleur, M.; Bloom, M.; Eikenberry, E. F.; Gruner, S. M.; Han, Y.; Cullis, P. R. Correlation between lipid plane curvature and lipid chain order. *Biophys. J.* **1996**, *70* (6), 2747−2757.

(80) Warschawski, D.; Devaux, P. Order parameters of unsaturated phospholipids in membranes and the effect of cholesterol: a 1H-13C solid-state NMR study at natural abundance. *Eur. Biophys. J.* **2005**, *34* (8), 987−96.

(81) Petrache, H. I.; Dodd, S. W.; Brown, M. F. Area per lipid and acyl length distributions in fluid phosphatidylcholines determined by (2)H NMR spectroscopy. *Biophys. J.* **2000**, *79* (6), 3172−92.

(82) Douliez, J. P.; Léonard, A.; Dufourc, E. J. Restatement of order parameters in biomembranes: calculation of C-C bond order parameters from C-D quadrupolar splittings. *Biophys. J.* **1995**, *68* (5), 1727−1739.

(83) Aussenac, F.; Laguerre, M.; Schmitter, J.-M.; Dufourc, E. J. Detailed structure and dynamics of bicelle phospholipids using selectively deuterated and perdeuterated labels. 2H NMR and molecular mechanics study. *Langmuir* **2003**, *19* (25), 10468−10479.

(84) Shaikh, S. R.; Brzustowicz, M. R.; Gustafson, N.; Stillwell, W.; Wassall, S. R. Monounsaturated PE does not phase-separate from the lipid raft molecules sphingomyelin and cholesterol: Role for polyunsaturation? *Biochemistry* **2002**, *41* (34), 10593−10602.

(85) Hitchcock, P. B.; Mason, R.; Thomas, K. M.; Shipley, G. G. Structural chemistry of 1,2 dilauroyl-DL-phosphatidylethanolamine: Molecular conformation and intermolecular packing of phospholipids. *Proc. Natl. Acad. Sci. U.S.A.* **1974**, *71* (8), 3036−3040.

(86) Seelig, A.; Seelig, J. Bilayers of dipalmitoyl-3-sn-phosphatidylcholine: Conformational differences between the fatty acyl chains. *Biochim. Biophys. Acta* **1975**, *406* (1), 1−5.

(87) Jämbeck, J. P. M.; Lyubartsev, A. P. An extension and further validation of an all-atomistic force field for biological membranes. *J. Chem. Theory Comput.* **2012**, *8* (8), 2938−2948.

(88) Senak, L.; Davies, M. A.; Mendelsohn, R. A quantitative IR study of hydrocarbon chain conformation in alkanes and phospholipids: CH2 wagging modes in disordered bilayer and HII phases. *J. Phys. Chem.* **1991**, *95* (6), 2565−2571.

(89) Moss, G. P. Basic terminology of stereochemistry. *Pure Appl. Chem.* **1996**, *68* (12), 2193−2222.

(90) Cates, D. A.; Strauss, H. L.; Snyder, R. G. Vibrational modes of liquid n-alkanes: Simulated isotropic raman spectra and band progressions for C5H12-C20H42 and C16D34. *J. Phys. Chem.* **1994**, *98* (16), 4482−4488.

N

dx.doi.org/10.1021/ct4010307 | *J. Chem. Theory Comput.* XXXX, XXX, XXX−XXX

(91) Snyder, R. G.; Strauss, H. L.; Elliger, C. A. C-H stretching modes and the structure of n-alkyl chains. 1. Long, disordered chains. *J. Phys. Chem.* **1982**, *86*, 5145−5150.

(92) Mendelsohn, R.; Senak, L. Quantitative determination of conformational disorder in biological membranes by FTIR spectroscopy. In *Biomolecular spectroscopy*; Clark, R. J. H. ,Hester, R. E., Eds.; Wiley: New York, 1993; pp 339−380.

(93) Casal, H. L.; McElhaney, R. N. Quantitative determination of hydrocarbon chain conformational order in bilayers of saturated phosphatidylcholines of various chain lengths by Fourier transform infrared spectroscopy. *Biochemistry* **1990**, *29* (23), 5423−5427.

(94) Tuchtenhagen, J.; Ziegler, W.; Blume, A. Acyl chain conformational ordering in liquid-crystalline bilayers: comparative FT-IR and 2H-NMR studies of phospholipids differing in headgroup structure and chain length. *Eur. Biophys. J.* **1994**, *23* (5), 323−335.

(95) Mendelsohn, R.; Davies, M. A.; Brauner, J. W.; Schuster, H. F.; Dluhy, R. A. Quantitative determination of conformational disorder in the acyl chains of phospholipid bilayers by infrared spectroscopy. *Biochemistry* **1989**, *28* (22), 8934−8939.

(96) Kučerka, N.; Gallová, J.; Uhríková, D.; Balgavý, P.; Bulacu, M.; Marrink, S.-J.; Katsaras, J. Areas of Monounsaturated Diacylphosphatidylcholines. *Biophys. J.* **2009**, *97* (7), 1926−1932.

(97) Ratto, T. V.; Longo, M. L. Obstructed diffusion in phase-separated supported lipid bilayers: A combined atomic force microscopy and fluorescence recovery after photobleaching approach. *Biophys. J.* **2002**, *83* (6), 3380−3392.

(98) Almeida, P. F. F.; Vaz, W. L. C.; Thompson, T. E. Lateral diffusion in the liquid phases of dimyristoylphosphatidylcholine/cholesterol lipid bilayers: a free volume analysis. *Biochemistry* **1992**, *31* (29), 6739−6747.

(99) Orädd, G.; Lindblom, G.; Westerman, P. W. Lateral diffusion of cholesterol and dimyristoylphosphatidylcholine in a lipid bilayer measured by pulsed field gradient NMR spectroscopy. *Biophys. J.* **2002**, *83* (5), 2702−2704.

(100) Filippov, A.; Orädd, G.; Lindblom, G. Influence of cholesterol and water content on phospholipid lateral diffusion in bilayers. *Langmuir* **2003**, *19* (16), 6397−6400.

(101) Vaz, W. L. C.; Clegg, R. M.; Hallmann, D. Translational diffusion of lipids in liquid crystalline phase phosphatidylcholine multibilayers. A comparison of experiment with theory. *Biochemistry* **1985**, *24* (3), 781−786.

(102) Scheidt, H. A.; Huster, D.; Gawrisch, K. Diffusion of cholesterol and its precursors in lipid membranes studied by 1H pulsed field gradient magic angle spinning NMR. *Biophys. J.* **2005**, *89* (4), 2504−2512.

(103) Kuśba, J.; Li, L.; Gryczynski, I.; Piszczek, G.; Johnson, M.; Lakowicz, J. R. Lateral diffusion coefficients in membranes measured by resonance energy transfer and a new algorithm for diffusion in two dimensions. *Biophys. J.* **2002**, *82* (3), 1358−1372.

(104) Jin, A. J.; Edidin, M.; Nossal, R.; Gershfeld, N. L. A singular state of membrane lipids at cell growth temperatures. *Biochemistry* **1999**, *38* (40), 13275−13278.

(105) Poger, D.; Mark, A. E. Lipid bilayers: The effect of force field on ordering and dynamics. *J. Chem. Theory Comput.* **2012**, *8* (11), 4807−4817.

(106) Wohlert, J.; Edholm, O. Dynamics in atomistic simulations of phospholipid membranes: Nuclear magnetic resonance relaxation rates and lateral diffusion. *J. Chem. Phys.* **2006**, *125* (20), 204703.

(107) Wang, Y.; Markwick, P. R. L.; de Oliveira, C. A. F.; McCammon, J. A. Enhanced lipid diffusion and mixing in accelerated molecular dynamics. *J. Chem. Theory Comput.* **2011**, *7* (10), 3199−3207.

(108) Basconi, J. E.; Shirts, M. R. Effects of temperature control algorithms on transport properties and kinetics in molecular dynamics simulations. *J. Chem. Theory Comput.* **2013**, *9* (7), 2887−2899.

(109) König, S.; Bayerl, T. M.; Coddens, G.; Richter, D.; Sackmann, E. Hydration dependence of chain dynamics and local diffusion in L-alpha-dipalmitoylphosphtidylcholine multilayers studied by incoherent quasi-elastic neutron scattering. *Biophys. J.* **1995**, *68* (5), 1871−1880.